Evolution of thermal crystal zonations and their heterogeneity in crystal populations during magma cooling

Cansu Culha[1,1], T Keller[2,2], and J Suckale[1,1]

[1]Stanford University
[2]University of Glasgow

November 30, 2022

Abstract

Crystal zonations provide valuable snapshot of the dynamic changes within a magma reservoir. However, there can be inconsistencies between crystals and their zonations, such that deciphering their signatures becomes convoluted. Crystals grow and shrink with temperature, pressure, and composition changes, which can change spatially and temporally as crystals transverse and evolve in the volcanic plumbing system. In this manuscript, we investigate how and at what spatial and temporal scales zonations record cooling processes in a magma lens after injection of fresh magma from depth. We simulate the cooling interface in either hot basaltic or dacitic magmas after their injection into a cold magma reservoir. We couple fluid dynamics to thermodynamics by allowing crystals with constant density and size to form and dissolve based on ambient melt properties and we resolve flow at the scale of each individual crystal. We infer zonations in our simulated crystals by tracking the temperatures they sample over time, but we do not grow or partially dissolve crystals. Our results show that when thermodynamics and fluid dynamics are coupled, a self-sustaining instability arises, because crystals transport the cooler-than-ambient melt in which they formed, creating conditions favorable to crystal formations where the crystal fraction is already high. Our results show that oscillatory zonation patterns can result from the self-sustaining instability, potentially overprinting larger, system-scale trends. Also, our results show that many of the crystals in the instability dissolve and lose their record of the instability. Many of the crystals that persist to the end of the simulation are shorter lived than the entire simulations, under estimating how long the domain remained at high temperatures. Our results suggest that zonations and their heterogeneity can be indicative of local instead of system scale processes, highlighting the importance of having multiple indicators to decipher a system scale process. Thus, we propose multiple indicators for the self-sustaining instability that we describe here.

1

Evolution of thermal crystal zonations and their heterogeneity in crystal populations during magma cooling

C. Culha[1], T. Keller[2], J. Suckale[1]

[1]Stanford University, Department of Geophysics, 397 Panama Mall, Stanford CA 94305, USA.
[2]University of Glasgow, School of Earth and Geographical Sciences, 8NN University Avenue, Glasgow G12 8QQ, UK.

Key Points:

- Coupling flow dynamics to thermal evolution and phase change results in a reactive crystal-driven instability.
- The instability can lead to crystal zonations, preserving temporal evolution, spatial heterogeneity and crystalline scale flow dynamics.
- Crystals that can record the nuances of the instability may underestimate the longevity of a cooling magmatic system.

Corresponding author: Cansu Culha, `cculha@stanford.edu`

Abstract

Crystal zonations provide valuable snapshot of the dynamic changes within a magma reservoir. However, crystal zonations are often heterogeneous down to the hand-sample scale, such that deciphering their signatures becomes convoluted. Crystals are reactively precipitated and dissolving as a function of temperature, pressure, and composition. In this manuscript, we investigate what temperature histories crystals experience in a magma lens after its injection into a cooler magma reservoir. We simulate the cooling interface in either hot basaltic or dacitic magmas after their injection into a cooler magma reservoir. We couple fluid dynamics to thermodynamics by resolving flow at the crystalline-scale and allowing crystals with constant density and size to precipitate and dissolve based on ambient melt properties. We infer zonations in our simulated crystals by tracking the magma temperatures they sample over time. Our results show that when thermodynamics and fluid dynamics are coupled, a reactive, crystal-driven instability arises, because the negative buoyancy of crystals pulls along the cooler-than-ambient melt in which they precipitated. As crystals continue to precipitate along the cooling boundary, the instability develops into a sustained convective flow. Our results show that crystals record complex and unique zonations in this crystalline-scale domain, suggesting that zonations and their heterogeneity can be indicative of local instead of system scale processes. Also, our results show that many of the crystals in the instability dissolve and lose their thermal record of the instability. These results highlight the challenges of deciphering system-scale process from crystalline data.

Plain Language Summary

Similar to tree rings, crystals tell a story of their past through their zonations. However, unlike trees, crystals are dynamic and can grow as well as shrink. In order to understand what zonation patterns a natural sample crystal would record during cooling, we built a simulator that is at the size of individuals crystals. We simulate the physics between crystals and melt, as well as, magma properties changing with temperature. Our results show that cooling a magmatic injection in a cold magma reservoir that precipitates denser than melt crystals can drive magma flow, which we call an instability. We can record the temperatures that a crystal samples over time, giving us insight into the zonations seen in natural sample crystals. Our results show that each crystal has a unique zonation that is dependent on the temperature distribution within its vicinity. Additionally, most of the crystals dissolve in the instability, so we lose their record. Overall, the crystals in our simulation can reproduce some of the confusing patterns that are often found in natural samples, suggesting that zonations can be deceiving. This result highlights the importance of using multiple indicators to understand a process at the scale of the volcano.

1 Introduction

Some volcanoes erupt with little or no clear warning, raising questions about what processes in the plumbing system trigger eruptions. Individual crystals in erupted samples may contain vital clues, because they tend to exhibit zonations indicative of changing conditions in the magma prior to eruption. These zonations manifest as variations in the chemical content along 1D profiles measured from crystal core to rim. Crystals grow or dissolve as a function of temperature (T), composition (C), and pressure (P) to maintain thermodynamic equilibrium with their surrounding magma, preserving a tabular history of the conditions in the volcanic plumbing systems over time (Ginibre et al., 2007; Cashman & Blundy, 2013; Wallace & Bergantz, 2005). Hence, crystal zonations hold clues about the inner structure and dynamic changes within a volcano (Vance, 1962; Ginibre et al., 2007; Cashman & Blundy, 2013; Wallace & Bergantz, 2005). Deciphering these clues, however, has proven challenging.

At system scale of an entire eruption or a layer in a plutonic outcrop, temperature, composition and pressure appear to be approximately homogeneous in many volcanic systems (Flynn & Mouginis-Mark, 1994; Whitney & Stormer, 1985; Bachmann et al., 2002). At the crystalline scale, individual crystals paint a different picture. For example, there is significant heterogeneity in the zonations of individual crystals at a range of scales. Even within a single sample, neighboring crystals may exhibit different zonations (Wallace & Berganz, 2005; Bachmann et al., 2002). Our aim is to advance our ability to reconstruct a coherent story from a heterogeneous crystal record through models designed particularly for that purpose.

Analyses of isotopic, trace, and chemical signatures along crystal zonations is advancing our ability to discriminate between the different contributions (T, P, $f\mathrm{O}_2$ and Comp.) that result in zonations (Cashman & Blundy, 2013; Cooper, 2019; Costa et al., 2020). Of these contributions, variability in temperature, or thermal zonations, has attracted particular attention as they may be related to eruption triggering mechanisms. While cooling zonations, or normal zonations, are to be expected for hot magma loosing heat to cooler wall rock, heating, or reverse zonations are also commonly observed. Some studies have argued that reverse zonations suggest that fresh injections of hotter, more mafic melt into cooler, more felsic, crystal-rich magma reservoirs may trigger eruptions (e.g. Cashman & Blundy, 2013; Murphy et al., 2000; Bachmann et al., 2002; Shane & Smith, 2013); other studies suggest that thermal zonations indicate latent heat release due to crystallization driven by degassing under decompression (Blundy et al., 2006) or evolving temperatures driven by large-scale thermal convection (e.g. Singer et al., 1995).

Many crystals in igneous rock samples show thermal zonations that evidence a dynamically evolving temperature in their host magma over time, but not all neighboring crystals show the same records of change. The heterogeneity in crystal populations indicates thermal variability over small spatial scales. Thermal convection was one of the first hypotheses proposed to explain crystal heterogeneity (e.g. Singer et al., 1995; Bachmann et al., 2002; Huber et al., 2009; Murphy et al., 2000), but it requires large magma reservoirs or low viscosities to sustain convection driven by thermal expansivity alone. Although plausible, recent studies of plutons highlight that melt-rich magma bodies likely exist as ephemeral, thin lenses within a larger—and much more viscous—crystal-rich mush zone. Another explanation of zonations is magma mingling following a mafic recharge (Sparks et al., 1977; Davidson & Tepley, 1997; Zellmer et al., 2003), a hypothesis that is supported by geologic evidence like mafic enclaves and schlieren features in intermediate to felsic igneous rocks (e.g., Alasino et al., 2019; Barbey et al., 2008). Yet, we currently lack a model that can explain the speed of mingling that is suggested by crystal observations (Till et al., 2015; Rae et al., 2016).

While thermal zonations have been studied a lot in more felsic and hence more explosive systems, thermal zonations also form in milder, more mafic eruptions. Volcanic sites like Hawaii and Stromboli are consistently erupting mafic magmas that can be traced back to a relatively homogeneous parent magma sourced from the mantle (e.g., Murata, 1970; Dupuy et al., 1981; Treiman, 1997). Even in these eruptions, heterogeneous thermal zonations in neighboring olivine and plagioclase crystal populations are well preserved (Kahl et al., 2011; Ruth et al., 2018), indicating that thermal zonations and heterogeneity at the crystalline scale are common signatures in many volcanic systems.

In our previous work (Culha et al., 2020), we simulate dense crystals unstably stratified in melt-rich magma. We observe crystals settling collectively at the layer scale but with small-scale variability arising from individual crystals moving relative to the collective flow. Here, we hypothesize that small-scale variability in flow within melt-rich magma lenses will result in complex thermal zonations in individual crystals as well as thermal zonation heterogeneity in the crystal population. In order to test our hypothesis, we develop a numerical model that captures the hydrodynamic interactions between crystals and melt, but also tracks the thermal evolution and allows for reactive crystal precip-

itation and dissolution. We couple our previous fluid mechanics model to a new model of thermal evolution with phase-change reactions—a coupled system we refer to as magma dynamics—by considering a magma of constant bulk composition but varying crystallinity, melt density, and viscosity as constrained by thermodynamic phase equilibria modeled with rhyolite-MELTS (Gualda et al., 2012; Ghiorso & Gualda, 2015). The model setup represents a hot, low-crystallinity, low-viscosity magma injected into a cool mush reservoir. Crystals denser than melt precipitating near the cooling interface are expected to settle collectively, thereby sustaining a crystal-driven flow instability of cooler magma sinking into the hot injection layer, over time developing into what we refer to as reactive crystal-driven convection.

In our simulations of reactive crystal-driven flow, we observe individual crystals sampling complex and locally heterogeneous thermal histories, suggesting that local-scale dynamics can create unique crystal zonations even for crystals involved in mesoscale collective flow patterns. Furthermore, systematic coupling between fluid mechanics and phase-change reaction leads to preservation bias of crystals only from certain flow histories. This result suggests that local-scale heterogeneity can overprint broader system-scale trends, highlighting the challenges of deducing system-scale dynamics from individual crystal records. In light of this result, we propose multiple indicators that in combination will allow better interpretation of magma dynamics from thermal zonation profiles.

2 Methods

To better understand the magma dynamics of coupled thermal evolution and reactive crystal-riven flow we formulate a model of a hot, melt-rich lens cooling after injection into a cooler mush body (Fig. 1A). We model this scenario as an idealised, two-dimensional, square domain of hot magma exposed to a cooler top boundary. To derive testable model predictions at the scale of individual crystals, we use a direct numerical simulation technique to resolve the precipitation of crystals near the cooling interface and their segregation into the adjacent melt-rich layer.
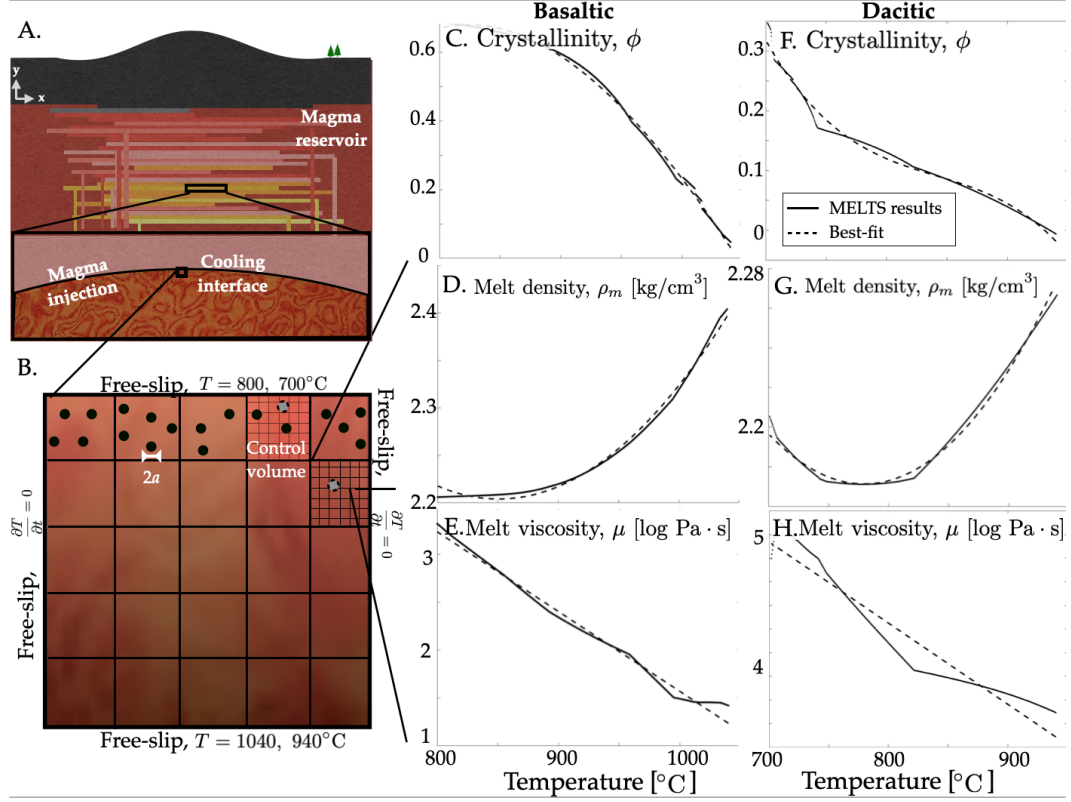
Our model is based on solving thermally coupled Stokes flow with crystals individually resolved as rigid, hydrodynamically interacting bodies. To maintain a crystallinity at equilibrium with the thermal evolution, we use a crystal population control algorithm that counts crystals present in a meso-scale control volume and adds/removes crystals in response to changing temperature (Fig. 1B). To capture small changes in crystallinity (Fig. 1C,F) yet resolve the dynamic subtleties in the domain arising from spatial variations in melt density and viscosity (Fig. 1D-E and G-H), we choose a control volume size that is 10 times larger than the crystal radius in both the lateral and vertical direction. This grid setup enables us to capture crystallinity differences of $\sim 2\%$. Below, we first describe the thermally coupled fluid mechanics model before introducing the algorithm used to maintain thermal phase equilibrium by adding and subtracting crystals in the control volume.

We solve for conservation of mass, momentum, and energy in a crystal-bearing, incompressible melt. Due to the sufficiently high viscosity of the melt, inertial effects are negligible and momentum conservation is reduced to the Stokes equation. We model both basaltic and dacitic magma (Table 1; Browne et al., 2006) as representative compositions, Fig. 1C–E and F–H, respectively, to highlight that our approach can be generalized to different compositions of mafic to felsic melt-rich systems. For simplicity, we ignore latent heat of crystallization. The governing equations for the melt phase are,

$$\nabla \cdot \mathbf{v}_\ell = 0 \tag{1}$$

$$\nabla P = \nabla \cdot \mu_\ell \left(\nabla \mathbf{v}_\ell + [\nabla \mathbf{v}_\ell]^T \right) + \rho_\ell \mathbf{g} + \mathbf{F}_c \tag{2}$$

$$\frac{\partial T}{\partial t} + \mathbf{v}_\ell \cdot \nabla T = \kappa \nabla^2 T \tag{3}$$

Figure 1.   rhyolite-MELTS results. We zoom into the cooling interface of a magma injection within a magma reservoir (A). We use basaltic and dacitic compositions to model phase equilibria for a range of temperatures at constant pressure to specify crystallinity (C and F), melt density (D and G) and melt viscosity (E and H) using the rhyolite-MELTS software. We update the crystallinity in a control volume of several grid cells by adding/removing crystals to match the calculated equilibrium, whereas we update the melt viscosity and density to their equilibrium value within individual grid cell (B). We use a different temperature range for basaltic composition from dacitic composition.

where t is time, $\mathbf{v}_\ell$ is the velocity of the melt, μ_ℓ is the melt viscosity, ρ_ℓ is the melt density, P is the melt pressure, $\mathbf{g}$ is gravity, $\mathbf{F_c}$ is the force exerted by the crystals on the liquid, c_p is the heat capacity, and $\kappa = k/\rho c_p$ the thermal diffusion coefficient. We take the heat capacity and conductivity of melt and crystal phases to be constant and the same at $c_p = 1367\text{J}/(\text{K·kg})$ and $k = 1.53\text{W}/(\text{m·K})$, respectively. The boundaries as shown in Fig. 1B are free slip ($\frac{\partial \mathbf{v}_\ell}{\partial \mathbf{n}} = \mathbf{0}$, $\mathbf{v}_\ell \cdot \mathbf{n} = \mathbf{0}$, $\frac{\partial P}{\partial \mathbf{n}} = 0$, where $\mathbf{n}$ is the vector normal to the boundary). The top and bottom temperatures of the domain are isothermal for basaltic and dacitic compositions. We take the hot and cold temperature values for basalt and compositions from Browne et al. (2006) as representative of typical basaltic and dacitic systems. The left and right walls are set to insulating ($\frac{\partial T}{\partial \mathbf{n}} = 0$). We set the initial temperature profile as,

$$T(y, \tilde{t} = 750s) = \frac{(T_t + T_b)}{2} - \frac{(T_b - T_t)}{2}\text{erf}\frac{(y - H)}{2\sqrt{\kappa \tilde{t}}} \tag{4}$$

where T_t and T_b are the initial top and bottom boundary temperatures, erf indicates the error function, H is the domain height, y is the vertical coordinate with initial uniformity in the x direction. Hence, the dynamic model sets in after heat has been lost diffusively for a time period $\tilde{t}$, an initial interval that would be nearly crystal-free and therefore without significant flow dynamics.

We assume that the crystal-free melt is Newtonian such that all non-linear effects apart from reactive coupling are a consequence of the resolved multiphase interactions. The governing equations for the crystal phase are Newton's equations of rigid-body motion

$$M_c \frac{d\mathbf{v}_c}{dt} = \mathbf{F}_c + M_c\mathbf{g} \tag{5}$$

$$\frac{d\left(\mathbf{I}_c \cdot \omega_c\right)}{dt} = \mathbf{T}_c \tag{6}$$

$$\frac{d\mathbf{X}_c}{dt} = \mathbf{v}_c \tag{7}$$

where M_c is the mass of an individual crystal, X_c is the crystal position at center of mass, $\mathbf{v_c}$ is the velocity of a crystal at center of mass, ω_c is the angular velocity of the crystal, $\mathbf{F}_c$ is the hydrodynamic force on crystals, $\mathbf{T}_c$ is the crystal torque resulting from the surrounding melt, and $\mathbf{I}_c$ is the moment of inertia tensor of a crystal.

For simplicity, we consider only a single type of crystal that is denser than the melt phase and has a constant radius, $a = 1$ mm. We set the crystal density to be a typical value for olivine $(3000\text{kg}/\text{m}^3)$ in the basaltic simulations and for plagioclase feldspar $(2600\text{kg}/\text{m}^3)$ in the dacitic simulations. The crystals conserve momentum at the wall boundary, but the high viscosity slows the crystals such that the crystals do not get into direct contact with the walls or with one another. To resolve the long-range hydrodynamic interactions between crystalline and melt phases, we use a customized, multiphase solver for magmatic systems that has been extensively bench-marked in previous studies (Suckale et al., 2012a; Qin & Suckale, 2016, 2017; Qin et al., 2019).

We use the thermodynamic equilibrium solver rhyolite-MELTS (Gualda et al., 2012; Ghiorso & Gualda, 2015) to obtain equilibrium phase proportions by volume, melt density, melt viscosity, and the evolution of melt and crystal compositions with temperature for a given magma bulk composition (Table 1), pressure (200 MPa) and oxygen fugacity (Nickel-nickel oxide) at the liquidus. We do not impose a fixed oxygen fugacity buffer for equilibrium calculations at different temperatures because there is no substantial evidence suggesting magma crystallises along a buffer (e.g. Borisov & Behrens, 2013; Borisov, 2016; O'Neill et al., 2006; Sack et al., 1980; Kress & Carmichael, 1991; Jayasuriya et al., 2004). In Fig. 1, we show the change in crystallinity (ϕ), melt density (ρ_m), and dynamic viscosity (μ) for the basaltic and dacitic bulk compositions as a function of temperature (T) together with best-fit polynomials which we use to more efficiently reference equilibrium calculations in our magma dynamics simulations.

Table 1. We base our compositions on the average compositions sampled by the Unzen eruption described in Browne et al. (2006). To estimate the basaltic composition, we use the mafic enclave composition. We created a line of best fit for each chemical content relative to SiO_2 content for the mafic enclave and the host magma. We use the reported SiO_2 content for the estimated basaltic and dacitic magma compositions Browne et al. (2006)and calculate the chemical compositions from the best fit. Then we normalize the compositions. The reported dacitic composition is the average composition.

| Comp.	SiO_2	TiO_2	Al_2O_3	Fe_2O_3	MnO	MgO	CaO	Na_2O	K_2O	P_2O_5	H_2O	T range	
Basalt	48.83	1.21	18.07	9.62	0.17	5.14	9.25	2.65	0.94	0.22	3.91	800-1040°C	
Dacite	63.92	0.62	15.16	0.82	0.08	2.04	4.28	3.47	2.52	0.17	3.87	700-940°C	

In a dynamically evolving magma body, phase segregation and thermal advection and diffusion act to locally disequilibrate phase proportions. In a natural system, disequilibrium will drive reactive equilibration by precipitating or dissolving crystals. Here, we model reactive phase change by an algorithm which instantaneously updates crystallinity to its equilibrium value in a control volume. We take the average temperature and crystallinity by volume over all of the cells in a control volume and compare to the equilibrium crystallinity at the given control volume temperature as given by rhyolite-MELTS (Fig. 1C–H). To enforce thermodynamic equilibrium, crystals of constant and equal size are randomly added or removed until the crystallinity is within less than one crystal per control volume of the equilibrium value. We refer to crystal removal and addition as "dissolution" and "precipitation" in the manuscript, respectively. For numerical stability reasons, there is a buffer of $2a$ size along the walls where crystals do not precipitate. Our software and all our runs can be accessed through our GitHub repository (Culha, 2020).

3 Instability initiates reactive, crystal-driven convection

To identify how a reactively evolving crystallinity interacts with flow dynamics, we compare two simulations with basaltic bulk compositions in Fig. 2. In one of the simulations, we maintain equilibrium crystallinity by precipitating or dissolving crystals during dynamic flow (Fig. 2A-C). We reference this simulation as the "reactive" simulation in the following. In the comparison simulation, we neglect equilibration by phase change and keep the number of crystals constant over time (Fig. 2D-F). We reference this simulation as the "non-reactive" simulation. The reactive simulation has melt density vary from 2200–2450 kg/m^3 and viscosity from 95–10^3 Pa·s as a function of T (Fig. 1D-E). The non-reactive simulation assumes a constant melt density of 2200 kg/m^3 and melt viscosity of 95 Pas.

The crystals in both simulations settle under the joint influence of gravity and the hydrodynamic forces arising from the presence of other crystals. The crystal-scale hydrodynamic interactions are important dynamically because they lead to spatially heterogeneous crystal motion relative to the collective flow pattern. We isolate and discuss this effect in detail in Culha et al. (2020). The crystals in the reactive simulation are heterogeneously distributed partly due to these hydrodynamic interactions and partly due to crystal precipitating in the cooler portions of the domain. In both simulations, the crystals present initially drag cold magma along as they settle collectively. In the non-reactive simulation, settling of the fixed number of crystals leaves behind a gap in crystal distribution along the boundary, whereas in the reactive simulation, where we enforce thermodynamic phase equilibrium, precipitation replenishes crystallinity along the cool-
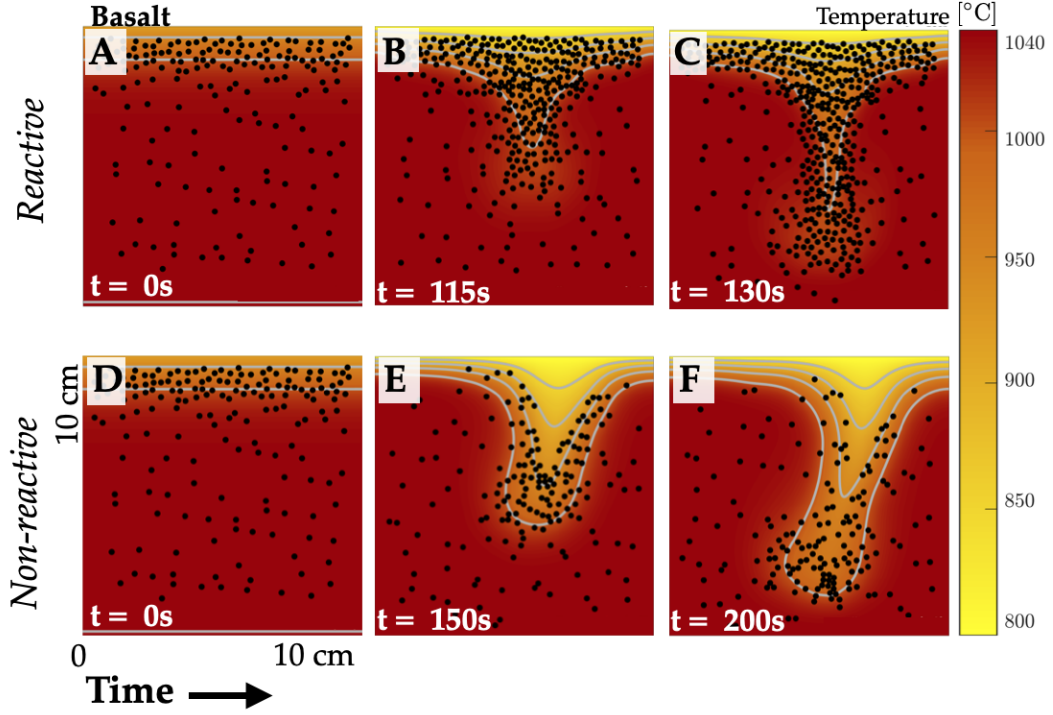
Figure 2. **Coupling flow dynamics to thermal evolution and crystal precipitation/dissolution leads to a reactive crystal-driven instability.** We show 2 simulations, one maintaining equilibrium by crystal population control during dynamic flow (A-C) and one without equilibration, where melt density and viscosity are held constant and the initial number of crystals is left to evolve without precipitation/dissolution (D-F). Both simulations start with the same initial crystallinity and identical crystal positions.

251 ing boundary layer, forming a reactive, crystal-driven instability (Fig. 2A-B) that grows
252 into the downward current of an emerging convective cell (Fig. 2C). The upward counter-
253 flow current is accommodated by the flow of crystal-poor magma.

254   Reactive equilibration coupled to dynamic flow precipitates crystals predominantly
255 where the developing instability is removing crystals from the cooling boundary layer,
256 thereby further enhancing the instability and sustaining convective flow. The reactive
257 crystal-driven convection advances crystals to 0.2m in 130s whereas the non-reactive crystal-
258 driven convection advances crystals to the same depth in 200s (Fig. 2). Although the
259 crystals rapidly travel in the reactive crystal-driven convection, the hottest gray contour
260 in the reactive simulation does not reach the depth that the hottest gray contour reaches
261 in the non-reactive simulation for the provided snapshots. Furthermore, the reactive, crystal-
262 driven instability shows a linear morphology, which is the result of its high crystallinity
263 and elevated interstitial melt viscosity that both resist deformation.

264   The simulations shown so far used the basaltic bulk composition. We compare these
265 results to the dacitic bulk composition to determine if this instability is widespread un-
266 der different conditions. One of the pertinent differences between basalt and dacite is
267 the melt viscosity, which is upwards of two orders of magnitude higher in the dacitic magma
268 (Fig. 1E,H). In Fig. 3, we compare snapshots of four simulations, two that include re-
269 active equilibration (A-B) and two that neglect phase change but differ in melt viscos-
270 ity by three orders of magnitude (C-D). To facilitate our analysis, we show the results
271 in non-dimensionalized form. We take the crystal radius, a, and the Stokes settling speed,
272 $\Delta v_s = \frac{2\Delta \rho a^2 g}{9\mu}$, as the characteristic size and speed.

273   Fig. 3A shows the same snapshot of the reactive basaltic simulation as Fig. 2C.
274 We compare this simulation to the reactive evolution of crystallinity using the dacitic
275 magma composition shown in Fig. 1 and Table 1. Dacitic magma crystals often record
276 cooler temperature ranges than basaltic magmas; hence we model the thermodynamics
277 at 700-940°C temperature range, while keeping the pressure the same as in the basaltic
278 run, which corresponds to the liquidus of the composition. At a similar non-dimensional
279 time, the reactive basaltic and dacitic simulations show very different results (Fig. 3A-
280 B). In the dacitic case (Fig. 3B), the domain crystallizes in a spatially homogeneous way
281 without forming a crystal-driven flow instability as in the basaltic case (Fig. 3A). We
282 show a snapshot that fully shows the domain to be covered in crystals as a comparison.
283 In contrast, in the non-reactive case the two magma compositions produce identical crys-
284 tal distributions and convective flow fields when observed at the same non-dimensional
285 time (Fig. 3C-D).

286   In the non-reactive simulations, the bulk density in the crystal rich layer is higher
287 than the crystal-poor layer below, because the melt density is constant throughout the
288 domain. The reactive instability arises even when we approximate neutral buoyancy of
289 the bulk magma density (e.g., we approximate the mixture of melt and crystal density
290 to stay constant between control volumes) which makes it different from the crystal driven
291 instabilities studied in laboratory settings (Kerr & Lister, 1992; Völtz et al., 2002; Mi-
292 chioka & Sumita, 2005; Shibano et al., 2013). The reactive, crystal-driven convection is,
293 to some degree, analogous to thermal convection, because lateral perturbations to av-
294 erage crystallinity and/or crystal settling can advance more rapidly than the cooling bound-
295 ary layer, driving convection. However, the unstable density stratification here is the con-
296 sequence of the local density contrast between crystals and melt, not a consequence of
297 the bulk density contrast due to thermal expansivity of the magma. Furthermore, crystal-
298 melt interactions introduce non-linear complexities within the collective flow that are not
299 present in idealised Rayleigh-Bénard convection.

300   The observed reactive, crystal-driven instability arises when the speed of collective
301 crystal settling exceeds the rate of diffusive growth of the thermal boundary layer. Con-
302 versely, if crystal settling is relatively slow, it will not keep pace with the diffusive bound-
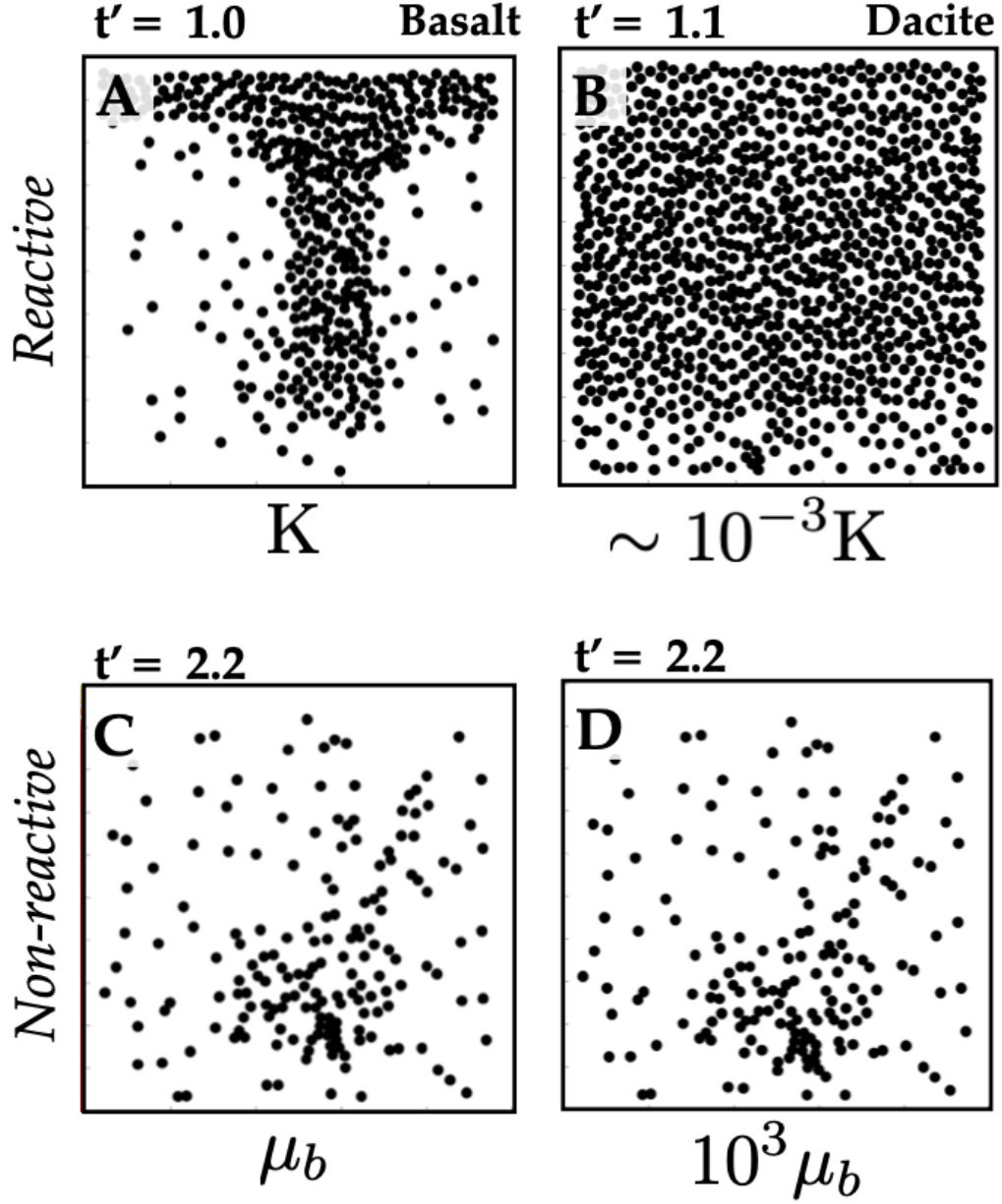
Figure 3. **High K hinders the instability.** Temporal snapshots of four simulations: two with (A-B), and two without reactive phase change (C-D). Simulations A and C as well as B and D start with the same initial crystallinity. We only increase the viscosity in D from C. We present our results in non-dimensional form.
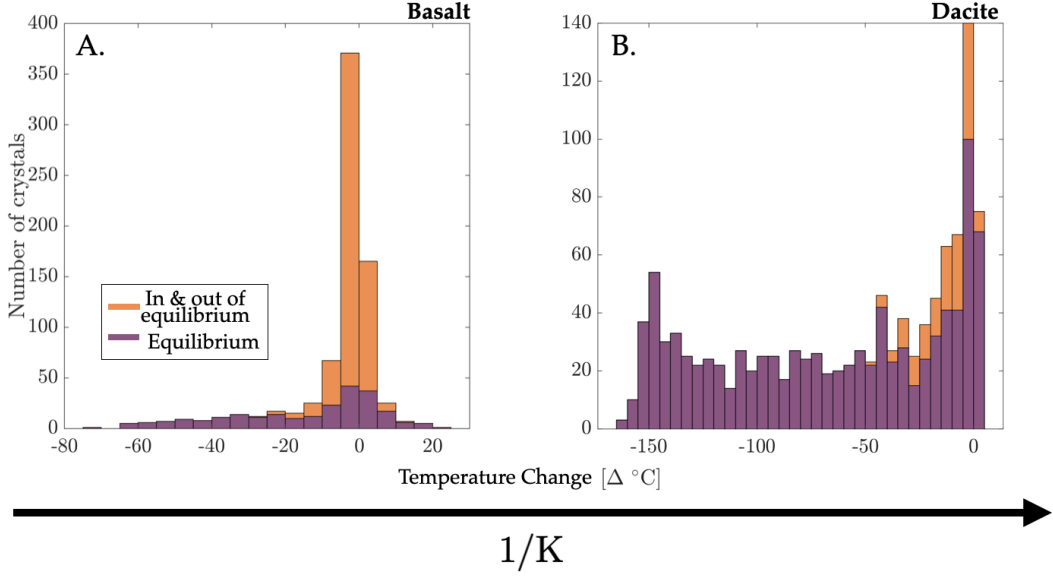
Figure 4. **Temperature changes for crystals in and out of equilibrium** Histogram of the temperature change between precipitation temperature and final crystal temperature for individual crystals during the two simulations in Fig. 3C-D. Histogram in A has crystals that precipitated throughout the simulation in Fig. 2A-C and C, whereas histogram in B has crystals that precipitated throughout the simulation in Fig. 3D. The purple histogram shows crystals that lasted to the end of the simulation snapshot in Fig. 3A-C and the orange histogram includes crystals that also dissolved during the simulation, "crystals out of equilibrium". For crystals that are out of equilibrium, the final crystal temperature is the temperature at which the crystal was last present.

ary growth, suppressing the growth of the instability. Thus, the differences between the reactively coupled basaltic and dacitic simulations arise due to competing speeds: (a) crystal-driven advection speed and (b) thermal diffusion speed. The ratio of these speeds determines if a reactive crystal-driven instability forms in magmatic settings.

The stability of reactive, crystal-driven convection can be characterised by a dimensionless number K analogous to a Rayleigh number as the ratio between the crystal settling speed and the thermal diffusion rate, but with the crystal size as the characteristic length scale and the crystal-melt density difference as the source of buoyancy contrast,

$$K = \frac{a^3 g (\rho_c - \rho_m)}{\kappa \mu}. \tag{8}$$

The K numbers for the reactive basaltic and dacitic simulations are $O(10^{-1})$ and $O(10^{-4})$, respectively. Our future research will analyze whether there is a critical K value for the onset of reactive crystal-driven convection.

4 Most crystals in reactive crystal-driven instability dissolve

Crystals entrained in convective flow may become disequilibrated with evolving thermal conditions. In our simulations, we instantaneously dissolve a crystal that is "out of equilibrium", in the sense that it has moved into a control volume where the average crystallinity now exceeds the calculated equilibrium value. In natural samples, crystals that are out of equilibrium initially have their rims dissolved and, with time, might dissolve

completely. While we do not model rim dissolution in our simulations directly, we can keep track of the thermal history of crystals regardless of whether they survived until the end of the simulation. We identify the temperature change of each of the crystals by recording its temperature at precipitation as well as the time of their dissolution or the stopping time of the simulation. In many cases, the crystals experience both cooling and heating temperature histories. Our metric is hence not necessarily identical to the maximum temperature range of a crystal's history.

In Fig. 4 we show the temperature change each crystal experiences over a temperature range of 240°C, the initial maximum temperature contrast within the simulation. Fig. 4A and B correspond to the reactive basaltic and dacitic simulations in Fig. 3A and B, respectively. We only record crystals that exist for at least two model output frames to compute a temperature difference. We show the crystals that last until the end of the simulation in purple regardless of when they formed and all of the crystals that existed for more than two model output frames throughout the simulation in orange. Although some of the crystals in the purple histogram might have entered into a control volume that was unfavorable for them, these crystals were not randomly chosen to dissolve in our algorithm. We label the crystals depicted in the purple histogram as crystals in "equilibrium" and the ones in orange as crystal "in and out of equilibrium".

In the reactive, basaltic simulation (Fig. 4A), the two histograms are different: at least 69% of the crystals in Fig. 4A precipitated and/or dissolved during the simulation. In the reactive, dacitic simulation (Fig. 4B), the two histograms are similar: only about 13% of the crystals in Fig. 4B dissolve during the simulation. Most crystals in the reactive, dacitic simulation stay in thermodynamic equilibrium, indicating a lesser degree of dynamic disequilibration in the absence of the flow instability. In comparison, Fig. 4A shows that most of the crystals in reactive crystal-driven instability go out of equilibrium, indicating a much higher degree of dynamic disequilibration. In natural samples, this likely translates to many crystals presenting partially dissolved rims, known as resorption zones (Ginibre et al., 2002). Completely dissolved crystals would, of course, not be recorded in natural samples at all. Either scenario implies a partial or full loss of thermal history recorded in crystal zonations.

5 Reactive, crystal-driven instability leads to thermal zonations

While both simulations in Figure 4 start with the same gradient in temperature of 240°C, 23% of the crystals in equilibrium experience net heating throughout their recorded history in Fig. 4A, whereas only 3% of the crystals in Fig. 4B show heating. Additionally, the crystals show a wide range of temperature changes. Natural crystal samples show evidence of cooling, or normal zonations, and heating, or reverse zonations, as well as heterogeneity in zonations across crystal populations. In order to compare the processes modelled here to normal and reverse zonations observed in crystal populations as well as the zonation heterogeneity in crystal populations, we analyse the results of a simulation that lasts for a longer period of time than in Fig. 2-4. We run a reactive, basaltic simulation on a domain that is three times the size of the simulation in Fig. 2A-C.

While the initial condition of the simulation is the same as in the previous, the larger domain allows for two crystal-rich instabilities to form in parallel, as shown in Fig. 5A-C. The one on the right advances relatively rapidly through the domain and the tip of the instability separates from the spine. To analyse a range of crystal histories evolving along distinct paths we select different sub-populations according to their initial and final positions and track their migration through the domain; these are highlighted in colour in Fig. 5. Most crystals in these sub-populations escape dissolution for the majority of the simulation. Blue and green crystals are initially positioned on the left and right sides of the cooling boundary layer, respectively, and remain within the top half of the domain over the course of the simulation. Purple crystals are a subgroup of the blue crystals that
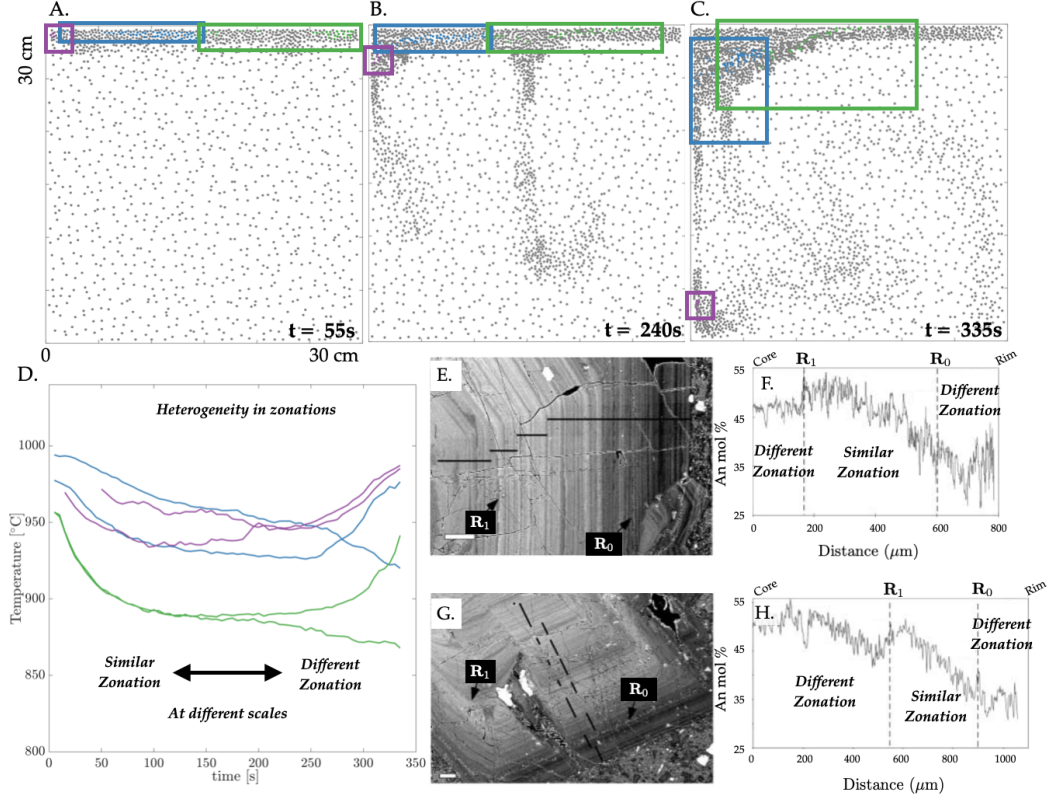
Figure 5. **Crystal displacement on scales comparable to crystal diameter may result in crystal zonations unique from the crystals in their immediate vicinity** A-C shows snapshots of a simulation with same initial conditions as the simulation in Fig. 2(A-C) but 3x the size of that in Fig. 2A-C. We highlight three crystal sub-populations to show how crystals move together in some regions and separate in others. Purple crystals are crystals that traveled to the bottom of the domain over the course of the simulation. Blue and green crystals precipitated in the left and right sides of the top domain, respectively, and remained in the top half of the domain during the portion of the dynamics shown here. The square box encapsulates all of the crystals in each category. D shows temperature profiles of crystals from A-C. We compare our results to natural crystal samples from Parinacota Volcano, Chile (Ginibre et al., 2002). The anorthite content zonations of E and G are in F and G. The gray dashed lines labeled R_1 and R_0 point to suspected resorption zones along the zonation.

reach the base of the domain within the simulation time. The colored squares encapsulate all of the crystals in each of the sub-populations. The different sub-populations reveal that crystals that start in close proximity, such as purple and blue crystals, can end in very different parts of the domain as a consequence of reactive crystal-driven flow. Conversely, crystals starting out in different segments of the domain can move closer to one another and even mix, such as the green and blue crystals.

Fig. 5D shows 2 crystals with detailed thermal crystal histories in each of the purple, blue and green sub-populations. We picked these 6 crystals to show how they can have both very different and similar thermal histories even though they neighbor one another. We record the average temperature of the cells in the crystal over time to record these thermal histories. This choice is a simplification, since in natural samples each crystal zone within its greater zonation is thought to sample the temperature of the melt that the crystal is equilibrating with along its rim.

The green sampled crystals record around the same temperature and similar cooling rates initially, but then one of them begins to record significant heating while the other shows continued cooling. The two blue crystals show similar cooling histories to the green ones, but they sample different initial temperatures and stay shifted in temperature. Similarly to samples from the green group, one blue crystal exhibits heating towards the end of the simulation, while the other continues to cool. The purple crystals, which remain close to each other throughout the simulation, initially have different precipitation temperatures and degrees of cooling/heating. However, as they founder collectively within the left instability, they sample similar temperatures towards the end of the run. These results show that crystals found next to one another may have experienced quite different temperature histories.

Furthermore, the crystals can experience short and rapid cooling and heating events which could resemble the heating and cooling experienced over longer times scales. For example, the rapid heating recorded by (a) the cooler of the two purple crystals between 100-200s and (b) the hotter of the two purple crystals between 50-75s and 100-150s can resemble the heating recorded by both the one blue, one green, and both purple crystals at 250-350s. Yet, these heating events are at different times in the history of the crystals and/or for different duration.

To illustrate the ramifications of these insights for the analysis of zonations, we reproduce observations of zonations in natural plagioclase samples from Ginibre et al. (2002) collected at the Parinacota Volcano, Chile, in Fig. 5E-H. We pick this study because it reveals the diversity of observed zonations in natural plagioclase crystals. In Fig. 5F and G, we reproduce the backscatter electron images and anorthite content measurements of two plagioclase crystals classified as having the same type of zonations (Ginibre et al., 2002). The original work identifies two resorption zones, R_0 and R_1, that mark the termination and onset, respectively, of zones in the plagioclase samples that have a similar pattern. In Fig. 6E-H, from the crystal core to R_1, the two crystals have different zones to one another: the crystal in F shows little variation in anorthite content whereas the crystal in H shows a general decrease in anorthite content. Although, between R_1 and R_0, the two crystals decrease in anorthite content to 35%, the length of the zone is different. Finally, between R_0 and the crystal rim, each of the crystals have a different degree of variability in anorthite content.

Temperature plays a key role in anorthite and trace element concentrations, such that a change in 10s of degrees Celsius can alter anorthite content by a few percent (Cashman & Blundy, 2013; Santo, 2005; Kojitani & Akaogi, 1995). This feature makes plagioclase a potentially valuable tracer for reactive crystal-driven convection. Since we do not model crystal growth in our simulations, we cannot compare simulation and data directly. Nevertheless, the thermal history identified in our simulations should be observable in the form of different growth zones for crystals like plagioclase. As shown in Fig. 5D, a crys-
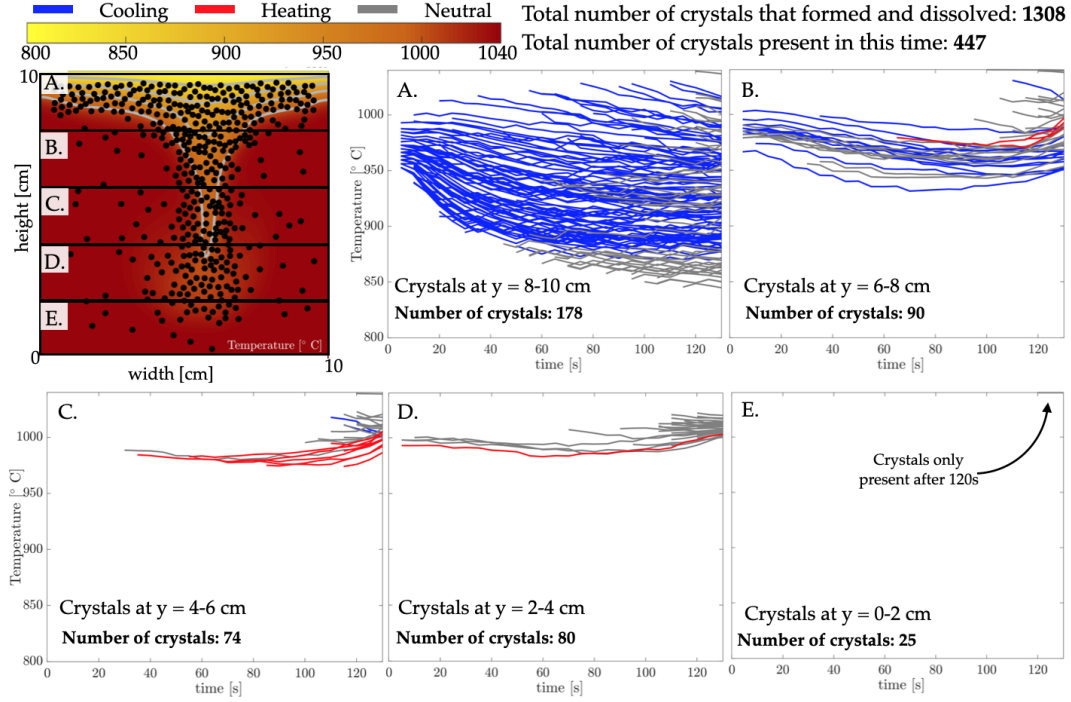
Figure 6. **Bias in our crystal analysis.** We show the final snapshot of the simulation in Fig. 2A-C. The instability is split into different segments and the thermal history of the crystals that terminate in that segment are shown in plots A-E. The blue, gray and red profiles suggest that the crystal experienced overall cooling, less than $10°C$ temperature change, or heating, respectively.

tal can initially have different zones and then experience similar zones (purple crystals) or similar zones and then transition into different zones (green crystals). A combination of our simulated thermal zonations could sandwich a similar zone between two different zones for multiple crystals like the natural plagioclase crystals in Fig. 5E-H. Another form of reproducing these results would be looking at different temporal scales of the crystalline history, such as in the example where the short lived, heating history of the cooler purple crystal at 50-75s resembles the longer-lived, heating of the one blue, one green, and both purple crystals.

Since we do not allow crystals to stay in the simulation once dissolved, we are not be able to capture any gaps in the crystal history analogous to a resorption zone. Simulating crystals to exist out of equilibrium and record resorption zones would allow the simulated crystals to last longer and show more varied zonations. Even with this limitation, our observations show that crystalline-scale flow can produce varied and heterogeneous thermal zonations that resemble natural plagioclase records.

6 Crystals provide an incomplete record of magma dynamics

Our analysis raises the question how well crystals testify to dynamically evolving conditions within a magmatic system. In Fig. 4, the orange histograms center around small temperature changes, whereas the purple histograms preserve a larger distribution of temperature changes. Our results suggest that the crystals that stay in equilibrium tell a different story than the crystals that have experienced disequilibration, inducing a bias in our crystal zonations analysis in Sec. 5. We specifically look at which parts of

the dynamics the crystals sample and which parts get omitted in their record of the instability. In Fig. 6 we split the instability into five segments. At the end of the simulation, we select all the crystals in each of the segments and display their thermal history for their entire lifetime. If the crystal experiences overall heating, cooling, or less than 10°C temperature change, then the profile is displayed in red, blue, or gray, respectively.

Since the cooler temperature at the top boundary locally increase melt viscosity, some of the crystals at the top of the instability move more slowly and cool with time (Fig. 6A). As a result, this part of the domain is well sampled and documented by the crystals that remain within the top segment, A. However, some information is lost about the crystals entrained in the instability, because some are subject to heating and dissolution and are hence removed from the simulation (Fig. 6B). The tip of the instability is least sampled by the crystal population and comprises crystals with the shortest life span, making it the most dynamic part of the instability (Fig. 6C-E). Our results show that there are two related, but distinct biases: (1) crystal growth does not fully sample the instability. Crystals preferentially precipitate at the tail of the instability (Fig. 6A) instead of at the tip (Fig. 6E) leading to a biased record of dynamic environments within the flow system; (2) crystal dissolution due to dynamic disequilibration will remove some growth rims or even entire crystals, and with them, their record of the magma dynamics.

7 Discussion

One of the fundamental challenges in volcanology is to infer the complex magmatic processes occurring at depth prior to eruption from limited data. Crystals trapped in magma quenched upon eruption record at least some aspects of the pre-eruptive conditions in the volcanic conduit directly (Demouchy & Mackwell, 2006; Spilliaert et al., 2006; DiBenedetto et al., 2020). However, leveraging crystal-scale data can be difficult since most volcanic models are formulated at the system scale of hundreds of metres to tens of kilometers and do not entail testable model predictions at the crystal scale that could be evaluated against this data.

Recent modeling efforts indicate that incomplete sampling can bias the interpretation of crystal populations if there is substantial heterogeneity in the zonations they record (Lilu et al., 2020; Andrews & Befus, 2020). This is consistent with our model findings. For example, all of our simulations model a system-scale cooling of a hotter magma injection, but some of the crystals record consistent heating or partial heating, which we interpret as corresponding to reverse zonations in natural data (Fig. 5D and 6). Our findings shed light on the processes contributing to this variability and identify inevitable gaps in the records of preserved crystal populations. Testing our process-based model against crystalline-scale observations might hence require multiple textural indicators in addition to chemical zonation patterns.

7.1 Indicators

In this section, we describe how the reactive, crystal-driven instability in melt rich systems could be reflected in zonations, glomerocrysts, crystal chains, and cross bedding to facilitate testing of our model results against field data. Here, we study reactive, crystal-driven convection only in the limit of relatively low average crystal fraction and infer the observational indicators of the simulated dynamics. In natural volcanic systems, crystals inevitably experience a much wider range of conditions than considered here, implying that the presence of the indicators discussed below may be suggestive of reactive, crystal-driven convection but offers no compelling proof of their uniqueness. Instead, our objective is to demonstrate an alternative explanation for some of the observed variability that does not entail a system-wide change in the dynamic.
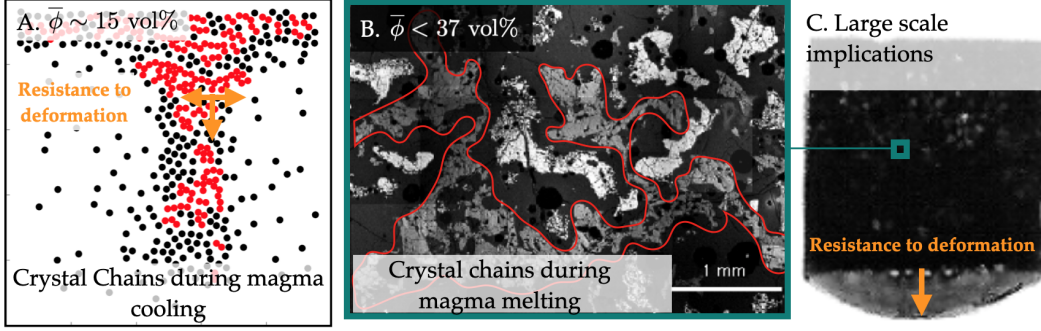
Figure 7. **Crystal chains at low crystallinity.** A is a snapshot of our simulation result as shown in Fig. 2C. The crystals in contact with neighboring crystals are colored red. There are horizontal and vertical crystal chains that form. Similar chains are found in the plagioclase crystals (in gray outlined in red of B) in the Holyoke Basalt Flow– originally published in Philpotts et al. (1998). C shows the experiment results from Philpotts et al. (1998). The hand sample data, of which B originated from, resists deformation when melted to have only 37 vol% crystallinity.

None of our simulations attempt to mimic a specific volcanic system, but our scaling analysis (Fig. 3) suggests that reactive, crystal-driven instabilities would form more readily in basaltic than dacitic systems. The reason is that the relatively lower viscosity of basaltic magma allows crystals of a wider range of sizes to move quickly with respect to the propagation speed of the cooling front. However, reactive, crystal-driven instabilities could occur in dacitic, or other more evolved, compositions as well, just over a different parameter range with potentially larger crystals. Another factor is the growth rate of crystals. Reactive, crystal-driven instabilities are particularly pronounced for mineral phases that grow and dissolve quickly and hence keep the system close to local phase equilibrium.

Our results suggest that crystals would be able to record reactive, crystal-driven instability as zonations (Fig. 5D and 6), depending on the speed of the instability and the crystal growth rate. Here, we assume that crystals adjust instantaneously to changing thermodynamic conditions, mimicking a fast-growing and fast-dissolving mineral phase. In addition to the growth rate, our simulations suggest that crystals in relatively low-viscosity, basaltic magma segregate quickly meaning they may experience relatively rapid changes in chemistry and temperature of their surrounding melt. In contrast, crystals in relatively high-viscosity, dacitic magma would experience more gradual changes in chemical content imprinted in their zonations. This expectation is consistent with some zonation patterns observed along plagioclase crystals in different magma compositions. For example, we identify at least 3 different plagioclase crystals in the Kutsugata basaltic lava in Rishire Volcano, Japan that jump in anorthite content on the order of 10s of per cent over a zonation thickness of 10s of micrometers (Fig. 6c,d, and f in (Kuritani, 1998)). In contrast, the plagioclase crystals in the dacitic Parinacota Volcano, Chile increase in anorthite content of less than 10 per cent over a zonation thickness of 100s of micrometers (Fig. 5F and H).

In addition to zonations, another observational signature of a reactive crystal-driven instability may be glomerocrysts, or crystal clusters. Crystals in a reactive crystal-driven instability congregate close to one another through "synneusis" (Culha et al., 2020; Schwindinger & Anderson, Jr., 1989; Vogt, 1921), the swimming together of crystals during flow. The process is captured in the non-reactive, basaltic simulation in Fig. 2D-F and is commonly

observed in the Stokes flow regime (Lamb, 1911; Batchelor & Batchelor, 2000; Qin & Suckale, 2020; DiBenedetto et al., 2020). In reactive crystal-driven flows, crystals also preferentially precipitate in crystal-rich regions along the top boundary and at the tail of the instability where cooling and crystal settling create favourable conditions (Fig. 6). Although we do not model different crystal types, our model suggests that crystals precipitating within the crystal-rich cluster of an established reactive crystal-driven instability would record the chemical signature of the residual melt, similar to the characteristics of crystals in the center of glomerocrysts (Garcia & Jacobson, 1979). We expect that the glomerocrysts would preserve a geochemical environment at their center that is distinct from the surrounding magma. Conversely, crystals along the outer rim would be most exposed to the dynamically changing geochemical environment and are most likely to experience resorption (Fig. 6C-E). Our simulations model early stages of cooling at high melt fractions. Although the high crystallinity of glomerocrysts might suggest their formation to be at later stages of cooling, our results suggest that they could form in early stages of cooling within melt-rich conditions, too. The crystal-rich segment of the instability is at 40 vol% crystallinity, although the average crystallinity of the entire domain is only 15 vol%. Our results would suggest that glomerocrysts could form prior to close packing of crystals. These results are consistent with observations that suggest formation of glomerocrysts prior to complete crystallization of melt (Hogan, 1993), but unclear if they also form prior to reaching a dense packing crystallinity of > 50 vol%.

Our results suggest that crystals may dynamically align in approximately linear chains during flow, as well. In Fig. 7A, we color crystals that are in less than half a radius proximity to other crystals in a single snapshot in red, highlighting the formation of transient, linear crystal chains. We observe chains forming within the crystal-rich instability, where crystallinity is considerably elevated above the average of 15 vol% over the entire domain.

One of the reasons why crystal chains matter is because they can transfer stress, or act as force chains (Schleicher & Bergantz, 2017; Sun et al., 2010; Sandnes et al., 2011; Qin et al., 2019; Qin & Suckale, 2020), and therefore provide resistance to deformation (Fig. 7C). We highlight a red lateral chain which appears to partially resist deformation. The highlighted features in our simulations are transient force chains; however if crystals remained aligned in chains for an extended period of time, they could inter-grow and continually transfer stress and resist deformation (DiBenedetto et al., 2020). Force chains are commonly observed in simulations at high crystal volume fractions (~50 vol%) (Bergantz et al., 2017); however, since analysis done by Philpotts et al. (in Philpotts et al., 1998, 1999), which showed force chains to form at crystallinities as low as 25 vol%, researchers have wondered how force chains could form at low crystallinities. Along with shear-induced flow at low crystallinity (Qin & Suckale, 2020), we interpret that force chains may also arise in reactive, crystal-driven instability where there is a heterogeneity in crystallinity ranging from $5 - 40$ vol%, while keeping the overall crystallinity at 15 vol%.

Another indicator of the reactive, crystal-driven instability at the base of the magmatic lens could be cross-bedded crystal layering. Our models show that the heads of crystal-rich instabilities may detach from their tails (e.g., Fig. 5C) and deliver crystals to the base of the magmatic lens in batches. In Fig. 5C, we show a snapshot of the instability with the purple crystals reaching the bottom of our simulation domain and the crystals spreading out. Unlike crystals individually "raining" through the magmatic lens, the collective settling of crystals in multiple distinct crystal-rich clusters would suggest a depositional environment similar to repeated gravity currents. This process may be preserved as cross-bedded crystal layers as observed at Duke Island, Skaergaard (Irvine, 1980) and Stillwater (Jackson, 1961) outcrops.

7.2 Implications

A system-scale implication of our results is that an instability at the crystal scale can enhance larger scale convective processes. For example, the results from our previous work (Culha et al., 2020) suggest that crystal-driven convection may add to other convective processes such as thermal (Singer et al., 1995; Bachmann et al., 2002; Huber et al., 2009; Murphy et al., 2000) or bubble-driven convection (Bergantz et al., 2017) driving mesoscale flow. Here, we show that crystal-driven instabilities become self-sustaining and faster when including reactive phase equilibration. Thus, thermodynamic phase changes could enhance other fluid dynamic instabilities. In fact, reactive, transport feed-backs are commonly studied features at the porous flow limit of magmatic systems that enhance melt transport (Keller et al., 2017; Mittal & Richards, 2017). Although our results show that the reactive, crystal-driven instability that we study here might be difficult to initiate in more felsic magmas (Fig. 3), precipitation and dissolution of crystals in convection driven by other processes will still occur and can further enhance convection.

The degree to which reactive, crystal-driven convection will enhance larger scale convection is dependent on how quickly crystals can respond to the new thermodynamic environment that they enter. Here, we make an explicit assumption that thermodynamic equilibrium is instantaneously met by precipitating new or dissolving pre-existing crystals. Hence, we provide an upper bound on how rapidly an instability may grow. Due to the kinetics of crystal nucleation and growth or dissolution, natural systems will have a slower response, and they may grow or resorb pre-existing crystals, altering the morphology of the instability we observe here. Better quantifying reaction, nucleation, and growth rates and introducing them into these models will lead to a more variable spectrum of reactive, crystal-driven instability and convection.

Our simulations provide a new perspective on interpretations of chemical zonations by associating crystal zonations with reactive, crystal-driven convection. Researchers have previously invoked large-scale, thermal convection, (e.g. Singer et al., 1995; Bachmann et al., 2002; Huber et al., 2009; Murphy et al., 2000), mafic injections (Annen et al., 2005), and magma mixing (Sparks et al., 1977; Davidson & Tepley, 1997; Zellmer et al., 2003) to explain crystal zonations in natural samples. Our simulations demonstrate that zonations do not necessarily represent system-scale processes, but may well capture crystalline-scale flow dynamics. For example, the local-scale flow that results from the dynamic nature of the reactive crystal-driven instability exposes our simulated crystals to changing thermal environments and introduces spatial heterogeneity, which is then recorded in their thermal histories.

In the absence of a system-scale overturn, processes like thermally- or bubble-driven flow, shearing, and small deformations can lead to local reordering of crystals which may appear like a new environment to a crystal. The size of the zonation will then depend on the longevity and speed of the force driving crystal reordering. Crystals not only record temporal evolution (Ubide & Kamber, 2018; Zellmer et al., 2003) and spatial heterogeneity (Roman et al., 2006; Kahl et al., 2011) of the magmatic system, but also local-scale dynamics as seen here. Our results suggest that crystal zonations for most crystals, especially quickly precipitating crystals like plagioclase, should be common, a prediction that is borne out by observations (Shore & Fowler, 1996). Hence, for certain types of crystals, the absence of zonations could be a more valuable observational constraint than the presence of zonations, because there are fewer dynamic scenarios their absence would be compatible with.

Our results suggest that for a given speed, relatively slow growing crystals would average over the nuances associated with the magma dynamics we study here, whereas relatively quickly growing crystals would be able to record more detailed histories. Yet, with similarly fast rates of dissolution, these crystals are also more prone to have their

record erased as resorption zones. Fig. 4A and 6 quantify how many and characterize where the majority of the crystals dissolve in a reactive, crystal-driven instability. This finding suggests that in natural samples, crystal zonation bands and entire crystals may dissolve due to dynamic disequilibration, erasing their record of a magmatic processes such as the reactive crystal-driven convection during cooling (Fig. 6). Hence, our results suggest that local-scale flow dynamics can overprint broader system-scale trends, highlighting the challenge of deducing system-scale dynamics from individual crystals.

Most of the sub-populations in the more dynamic region of our domain (melt-rich; Fig. 6B-E) are shorter lived than the entire simulation. Sampling these crystals with short residence times would suggest that the simulation was ephemeral. Underestimating the cooling rate from zonations has significant implications for interpreting magma storage timescales and temperatures. Recent literature on magma storage look at plagioclase and zircon crystals to understand timescales and temperatures of magma storage and notice surprisingly short timescales of magma storage in predominantly melt-rich, or hot, conditions (Cooper & Kent, 2014; Rubin et al., 2017).

Our results would suggest that rapidly precipitating and dissolving crystal zonation records, like plagioclase crystals, bias the interpretation of hot storage time to be much shorter than it may actually be. Consequently, the time between mobilization of a magma body and eruption may be longer than the 100s of years the plagioclase crystals appear to indicate (Cooper & Kent, 2014). Our results further emphasize the need to do process-based modeling of magmatic systems and analyze their implications at the crystalline scale to better interpret geochemical observations at the same scale (Gelman et al., 2013; Barboni et al., 2016; Kent & Cooper, 2018). By understanding the limits on the interpretation of crystalline data, we can more accurately quantify the longevity of hot storage regions, speed of remobilization, and rates of mafic injections that may drive eruptions.

8 Conclusion

Our study quantifies the thermal heterogeneity in crystal-scale data that will arise from phase change reactions in response to thermal disequilibration by dynamic flow. By resolving the crystal-melt interactions within a reacively evolving crystal load, we identify a self-sustaining instability driven by crystallization within a cooling boundary layer, which we call a reactive, crystal-driven instability. The collectively settling crystals in the instability drag cool melt from the interface into the hotter magma below. The instability develops into a reactive crystal-driven convection, resulting in a heterogeneous distribution of temperature, melt density, viscosity, and magma crystallinity throughout the magma lens. We find that the ratio of crystal advection speed and thermal diffusion speed, similar to a Rayleigh number, will determine if the instability forms in natural systems, and the instability is more likely to arise in basaltic compositions at the sub-metre scale, where crystal settling is faster than thermal diffusion.

The main contribution of our simulator is that it can track crystals and the thermal conditions that they sample, while allowing for crystal precipitation and dissolution. The crystal populations show a wide range of thermal zonations including heating, cooling, and oscillations, which resemble crystal zonations in natural samples. Moreover, we can keep record of the crystals that dissolve in our simulations, which make up the majority of the crystals entrained in the reactive, crystal-driven instability. Hence, the crystal population left over from reactive, crystal-driven instability does not provide a complete record of the flow dynamics that have occurred in the system. Our work firmly emphasizes the significance of using multiple geochemical and textural indicators in magmatic systems to decipher the processes creating the observable zonations in crystals.

Acknowledgments

The authors would like to thank Christy Till, Gail Mahood, Ayla Pamukcu and David Pollard for fruitful discussions throughout the development of the project. CC acknowledges support from the NSF's GRFP, Stanford University's McGee Grant and Stanford University's Lieberman Fellowship. TK acknowledges support from the Swiss National Science Foundation's Postdoc.Mobility Fellowship 177816. See our Github repository here for the Fortran simulator producing each case, some videos and the Matlab scripts that help generate the figures (Culha, 2020): `https://doi.org/10.5281/zenodo.4393097`.

References

Alasino, P. H., Ardill, K., Stanback, J., Paterson, S., Galindo, C., & Leopold, M. (2019). Magmatically folded and faulted schlieren zones formed by magma avalanching in the sonora pass intrusive suite, sierra nevada, california. *Geosphere*, *15*(5), 1677–1702.

Andrews, B. J., & Befus, K. S. (2020). Supersaturation nucleation and growth of plagioclase: a numerical model of decompression-induced crystallization. *Contributions to Mineralogy and Petrology*, *175*(3), 1–20.

Annen, C., Blundy, J., & Sparks, R. (2005). The genesis of intermediate and silicic magmas in deep crustal hot zones. *Journal of Petrology*, *47*(3), 505–539.

Bachmann, O., Dungan, M. A., & Lipman, P. W. (2002). The fish canyon magma body, san juan volcanic field, colorado: rejuvenation and eruption of an upper-crustal batholith. *Journal of Petrology*, *43*(8), 1469–1503.

Barbey, P., Gasquet, D., Pin, C., & Bourgeix, A. L. (2008). Igneous banding, schlieren and mafic enclaves in calc-alkaline granites: The Budduso pluton (Sardinia). *Lithos*, *104*(1-4), 147–163. doi: 10.1016/j.lithos.2007.12.004

Barboni, M., Boehnke, P., Schmitt, A. K., Harrison, T. M., Shane, P., Bouvier, A.-S., & Baumgartner, L. (2016). Warm storage for arc magmas. *Proceedings of the National Academy of Sciences*, *113*(49), 13959–13964.

Batchelor, C. K., & Batchelor, G. (2000). *An introduction to fluid dynamics*. Cambridge university press.

Bergantz, G. W., Schleicher, J. M., & Burgisser, A. (2017). On the kinematics and dynamics of crystal-rich systems. *Journal of Geophysical Research: Solid Earth*, *122*(8), 6131–6159.

Blundy, J., Cashman, K., & Humphreys, M. (2006). Magma heating by decompression-driven crystallization beneath andesite volcanoes. *Nature*, *443*(7107), 76–80.

Borisov, A. (2016). Mutual interaction of redox pairs in silicate melts: equilibria involving metallic phases. *Petrology*, *24*(2), 117–126. Retrieved from `http://link.springer.com/10.1134/S0869591116020028` doi: 10.1134/S0869591116020028

Borisov, A., & Behrens, H. (2013). The effect of titanium and phosphorus on ferric / ferrous ratio in silicate melts : an experimental study. *Contrib. Miner. Pet.*, *166*, 1577–1591. doi: 10.1007/s00410-013-0943-9

Browne, B. L., Eichelberger, J. C., Patino, L. C., Vogel, T. A., Dehn, J., Uto, K., & Hoshizumi, H. (2006). Generation of Porphyritic and Equigranular mafic enclaves during magma recharge events at Unzen volcano, Japan. *J. Petrol.*, *47*(2), 301–328. doi: 10.1093/petrology/egi076

Cashman, K., & Blundy, J. (2013). Petrological cannibalism: the chemical and textural consequences of incremental magma body growth. *Contributions to Mineralogy and Petrology*, *166*(3), 703–729.

Cooper, K. M. (2019). Time scales and temperatures of crystal storage in magma reservoirs: Implications for magma reservoir dynamics. *Philosophical Transactions of the Royal Society A*, *377*(2139), 20180009.

Cooper, K. M., & Kent, A. J. (2014). Rapid remobilization of magmatic crystals kept in cold storage. *Nature*, *506*(7489), 480–483.

Costa, F., Shea, T., & Ubide, T. (2020). Diffusion chronometry and the timescales of magmatic processes. *Nature Reviews Earth & Environment*, 1–14.

Culha, C. (2020, Dec). Reactive, multi-phase, fluid dynamics software. Retrieved from https://doi.org/10.5281/zenodo.4393097

Culha, C., Suckale, J., Keller, T., & Qin, Z. (2020). Crystal fractionation by crystal-driven convection. *Geophysical Research Letters*, *47*(4), e2019GL086784. doi: 10.1029/2019GL086784

Davidson, J. P., & Tepley, F. J. (1997). Recharge in volcanic systems: evidence from isotope profiles of phenocrysts. *Science*, *275*(5301), 826–829.

Demouchy, S., & Mackwell, S. (2006). Mechanisms of hydrogen incorporation and diffusion in iron-bearing olivine. *Phys. Chem. Miner.*, *33*(5), 347–355. doi: 10.1007/s00269-006-0081-2

DiBenedetto, M., Qin, Z., & Suckale, J. (2020). Crystal aggregates record the pre-eruptive flow field in the volcanic conduit at kīlauea, hawaii. *Science Advances*, *6*(49), eabd4850.

Dupuy, C., Dostal, J., Girod, M., & Liotard, M. (1981). Origin of volcanic rocks from stromboli (italy). *Journal of Volcanology and Geothermal Research*, *10*(1-3), 49–65.

Flynn, L. P., & Mouginis-Mark, P. J. (1994). Temperature of an active lava channel from spectral measurements, kilauea volcano, hawaii. *Bulletin of Volcanology*, *56*(4), 297–301.

Garcia, M. O., & Jacobson, S. S. (1979). Crystal clots, amphibole fractionation and the evolution of calc-alkaline magmas. *Contributions to Mineralogy and Petrology*, *69*(4), 319–327.

Gelman, S. E., Gutiérrez, F. J., & Bachmann, O. (2013). On the longevity of large upper crustal silicic magma reservoirs. *Geology*, *41*(7), 759–762.

Ghiorso, M. S., & Gualda, G. A. R. (2015). An H₂O â CO₂ mixed fluid saturation model compatible with rhyolite â MELTS. *Contrib. to Mineral. Petrol.*, *169*(6), 1–30. doi: 10.1007/s00410-015-1141-8

Ginibre, C., Wörner, G., & Kronz, A. (2002). Minor-and trace-element zoning in plagioclase: implications for magma chamber processes at parinacota volcano, northern chile. *Contributions to Mineralogy and Petrology*, *143*(3), 300–315.

Ginibre, C., Wörner, G., & Kronz, A. (2007, 08). Crystal Zoning as an Archive for Magma Evolution. *Elements*, *3*(4), 261-266. Retrieved from https://doi.org/10.2113/gselements.3.4.261 doi: 10.2113/gselements.3.4.261

Gualda, G. A. R., Ghiorso, M. S., Lemons, R. V., & Carley, T. L. (2012). Rhyolite-MELTS : a Modified Calibration of MELTS Optimized for Silica-rich, Fluid-bearing Magmatic Systems. *J. Petrol.*, *53*(5), 875–890. doi: 10.1093/petrology/egr080

Hogan, J. P. (1993). Monomineralic glomerocrysts: textural evidence for mineral resorption during crystallization of igneous rocks. *The Journal of geology*, *101*(4), 531–540.

Huber, C., Bachmann, O., & Manga, M. (2009). Homogenization processes in silicic magma chambers by stirring and mushification (latent heat buffering). *Earth and Planetary Science Letters*, *283*(1-4), 38–47.

Irvine, T. (1980). Magmatic density currents and cumulus processes. *American Journal of Science*, *280*(Jackson Volume), 1–58.

Jackson, E. (1961). Primary textures and mineral associations in the ultramafic zone of the stillwater complex, montana: Us geol. survey prof. paper 358, 106 p. 1963, chromium. *23rd Session, Sec*, *1*, 135–140.

Jayasuriya, K. D., OÊŒNeill, H. S., Berry, A. J., & Campbell, S. J. (2004). A Mössbauer study of the oxidation state of Fe in silicate melts. *Am. Mineral.*, *89*(1991), 1597–1609.

Kahl, M., Chakraborty, S., Costa, F., & Pompilio, M. (2011). Dynamic plumbing system beneath volcanoes revealed by kinetic modeling, and the connection to monitoring data: An example from mt. etna. *Earth and Planetary Science Letters*, *308*(1-2), 11–22.

Keller, T., Katz, R. F., & Hirschmann, M. M. (2017). Volatiles beneath mid-ocean ridges: Deep melting, channelised transport, focusing, and metasomatism. *Earth and Planetary Science Letters*, *464*, 55–68.

Kent, A. J., & Cooper, K. M. (2018). How well do zircons record the thermal evolution of magmatic systems? *Geology*, *46*(2), 111–114.

Kerr, R. C., & Lister, J. R. (1992). Further results for convection driven by the differential sedimentation of particles. *Journal of Fluid Mechanics*, *243*, 227–245.

Kojitani, H., & Akaogi, M. (1995). Measurement of heat of fusion of model basalt in the system diopside-forsterite-anorthite. *Geophysical research letters*, *22*(17), 2329–2332.

Kress, V. C., & Carmichael, I. S. E. (1991). The compressibility of silicate liquids containing Fe2O3 and the effect of composition, temperature, oxygen fugacity and pressure on their redox states. *Contrib. to Mineral. Petrol.*, *108*(1-2), 82–92. doi: 10.1007/BF00307328

Kuritani, T. (1998). Boundary layer crystallization in a basaltic magma chamber: evidence from rishiri volcano, northern japan. *Journal of Petrology*, *39*(9), 1619–1640.

Lamb, H. (1911). Xv. on the uniform motion of a sphere through a viscous fluid. *The London, Edinburgh, and Dublin Philosophical Magazine and Journal of Science*, *21*(121), 112–121.

Lilu, C., Costa, F., & Bergantz, G. (2020). Linking fluid dynamics and olivine crystal scale zoning during simulated magma intrusion. *Contributions to Mineralogy and Petrology*, *175*(6).

Michioka, H., & Sumita, I. (2005). Rayleigh-Taylor instability of a particle packed viscous fluid: Implications for a solidifying magma. *Geophys. Res. Lett.*, *32*(3), 1–4. doi: 10.1029/2004GL021827

Mittal, T., & Richards, M. A. (2017). Plume-ridge interaction via melt channelization at g alápagos and other near-ridge hotspot provinces. *Geochemistry, Geophysics, Geosystems*, *18*(4), 1711–1738.

Murata, K. (1970). Tholeiitic basalt magmatism of kilauea and mauna loa volcanoes of hawaii. *Naturwissenschaften*, *57*(3), 108–113.

Murphy, M., Sparks, R., Barclay, J., Carroll, M., & Brewer, T. (2000). Remobilization of andesite magma by intrusion of mafic magma at the soufriere hills volcano, montserrat, west indies. *Journal of petrology*, *41*(1), 21–42.

O'Neill, H. S. C., Berry, A. J., McCammon, C. C., Jayasuriya, K. D., Campbell, S. J., & Foran, G. (2006). An experimental determination of the effect of pressure on the Fe3/âFe ratio of an anhydrous silicate melt to 3.0 GPa. *Am. Mineral.*, *91*(2-3), 404–412. doi: 10.2138/am.2005.1929

Philpotts, A. R., Brustman, C. M., Shi, J., Carlson, W. D., & Denison, C. (1999). Plagioclase-chain networks in slowly cooled basaltic magma. *Am. Mineral.*, *84*(11-12), 1819–1829. doi: 10.2138/am-1999-11-1209

Philpotts, A. R., Shi, J., & Brustman, C. (1998). Role of plagioclase crystal chains in the differentiation of partly crystallized basaltic magma. *Nature*, *395*(6700), 343–346.

Qin, Z., Alison, K., & Suckale, J. (2019). Rotation matters-direct numerical simulations of rectangular particles in suspensions at low to intermediate solid fraction. *arXiv preprint arXiv:1903.08167*.

Qin, Z., & Suckale, J. (2016). A virtual laboratory for three-phase flow : 1 . Direct numerical simulations of bubble-crystal interactions in basaltic suspensions. , 1–60.

840 Qin, Z., & Suckale, J. (2017). Direct numerical simulations of gasâsolidâliquid inter-
841   actions in dilute fluids. *Int. J. Multiph. Flow*, *96*(November), 34–47.
842 Qin, Z., & Suckale, J. (2020). Flow-to-sliding transition in crystal-bearing magma.
843   *Journal of Geophysical Research: Solid Earth*, *125*(2), e2019JB018549.
844 Rae, A. S. P., Edmonds, M., Maclennan, J., Morgan, D., Houghton, B., Hartley,
845   M. E., & Sides, I. (2016). Time scales of magma transport and mixing at
846   K??lauea Volcano, Hawai'i. *Geology*, *44*(6), 463–466. doi: 10.1130/G37800.1
847 Roman, D. C., Cashman, K. V., Gardner, C. A., Wallace, P. J., & Donovan, J. J.
848   (2006). Storage and interaction of compositionally heterogeneous magmas from
849   the 1986 eruption of augustine volcano, alaska. *Bulletin of Volcanology*, *68*(3),
850   240–254.
851 Rubin, A. E., Cooper, K. M., Till, C. B., Kent, A. J., Costa, F., Bose, M., . . . Cole,
852   J. (2017). Rapid cooling and cold storage in a silicic magma reservoir recorded
853   in individual crystals. *Science*, *356*(6343), 1154–1156.
854 Ruth, D. C., Costa, F., de Maisonneuve, C. B., Franco, L., Cortés, J. A., & Calder,
855   E. S. (2018). Crystal and melt inclusion timescales reveal the evolution of
856   magma migration before eruption. *Nature communications*, *9*(1), 1–9.
857 Sack, R. O., Carmichael, I. S. E., Rivers, M., & Ghiorso, M. S. (1980). Contribu-
858   tions to mineralogy and petrology Ferric-Ferrous equilibria in natural silicate
859   liquids at 1 bar. *Contrib. Miner. Pet.*, *75*, 369–376.
860 Sandnes, B., Flekkøy, E., Knudsen, H., Måløy, K., & See, H. (2011). Patterns and
861   flow in frictional fluid dynamics. *Nature communications*, *2*(1), 1–8.
862 Santo, A. (2005). Magmatic evolution processes as recorded in plagioclase phe-
863   nocrysts of nea kameni rocks (santorini volcano, greece). In M. Fytikas &
864   G. E. Vougioukalakis (Eds.), *The south aegean active volcanic arc* (Vol. 7,
865   p. 139 - 160). Elsevier. Retrieved from `http://www.sciencedirect.com/`
866   `science/article/pii/S1871644X05800361`   doi: https://doi.org/10.1016/
867   S1871-644X(05)80036-1
868 Schleicher, J., & Berganz, G. (2017). The mechanics and temporal evolution of an
869   open-system magmatic intrusion into a crystal-rich magma. *Journal of Petrol-*
870   *ogy*, *58*(6), 1059–1072.
871 Schwindinger, K. R., & Anderson, Jr., A. T. (1989). Synneusis of Kilauea Iki
872   olivines. *Contrib. Miner. Pet.*, *103*, 187—-198.
873 Shane, P., & Smith, V. C. (2013). Using amphibole crystals to reconstruct magma
874   storage temperatures and pressures for the post-caldera collapse volcanism at
875   okataina volcano. *Lithos*, *156*, 159–170.
876 Shibano, Y., Sumita, I., & Namiki, A. (2013). A laboratory model for melting ero-
877   sion of a magma chamber roof and the generation of a rhythmic layering. *J.*
878   *Geophys. Res. Solid Earth*, *118*(8), 4101–4116. doi: 10.1002/jgrb.50295
879 Shore, M., & Fowler, A. D. (1996). Oscillatory zoning in minerals; a common phe-
880   nomenon. *The Canadian Mineralogist*, *34*(6), 1111–1126.
881 Singer, B. S., Dungan, M. A., & Layne, G. D. (1995). Textures and Sr, Ba, Mg, Fe,
882   K, and Ti compositional profiles in volcanic plagioclase: Clues to the dynamics
883   of calc-alkaline magma chambers. *Am. Mineral.*, *80*, 776–798.
884 Sparks, Sigurdsson, H., & Wilson, L. (1977). Magma mixing: a mechanism
885   for triggering acid explosive eruptions. *Nature*, *267*(5609), 315–318. Re-
886   trieved from `http://www.nature.com/nature/journal/v267/n5609/abs/`
887   `267315a0.html{\%}5Cnpapers2://publication/uuid/1D841CE7-BD35-4AC5`
888   `-8560-46844B6AF96B{\%}5Cnhttp://www.nature.com/doifinder/10.1038/`
889   `267315a0`   doi: 10.1038/267315a0
890 Spilliaert, N., Allard, P., Métrich, N., & Sobolev, A. (2006). Melt inclusion record of
891   the conditions of ascent, degassing, and extrusion of volatile-rich alkali basalt
892   during the powerful 2002 flank eruption of mount etna (italy). *Journal of*
893   *Geophysical Research: Solid Earth*, *111*(B4).
894 Suckale, J., Sethian, J., Yu, J., & Elkins-Tanton, L. (2012a). Crystals stirred

up: 1. direct numerical simulations of crystal settling in nondilute magmatic suspensions. *Journal of Geophysical Research: Atmospheres*, *117*(8). doi: 10.1029/2012JE004066

Sun, Q., Jin, F., Liu, J., & Zhang, G. (2010). Understanding force chains in dense granular materials. *International Journal of Modern Physics B*, *24*(29), 5743–5759.

Till, C. B., Vazquez, J. A., & Boyce, J. W. (2015). Months between rejuvenation and volcanic eruption at yellowstone caldera, wyoming. *Geology*, *43*(8), 695–698.

Treiman, A. H. (1997). The parent magmas of the cumulate eucrites: A mass balance approach. *Meteoritics & Planetary Science*, *32*(2), 217–230.

Ubide, T., & Kamber, B. S. (2018). Volcanic crystals as time capsules of eruption history. *Nature communications*, *9*(1), 1–12.

Vance, J. A. (1962). Zoning in igneous plagioclase; normal and oscillatory zoning. *American Journal of Science*, *260*(10), 746–760.

Vogt, J. H. L. (1921). The physical chemistry of the crystallization and magmatic differentiation of igneous rocks. *The Journal of Geology*, *29*(4), 318–350.

Völtz, C., Pesch, W., & Rehberg, I. (2002). Rayleigh-Taylor instability in a sedimenting suspension. *Phys. Rev. E - Stat. Physics, Plasmas, Fluids, Relat. Interdiscip. Top.*, *65*(1), 1–7. doi: 10.1103/PhysRevE.65.011404

Wallace, G. S., & Bergantz, G. W. (2005). Reconciling heterogeneity in crystal zoning data: An application of shared characteristic diagrams at Chaos Crags, Lassen Volcanic Center, California. *Contrib. to Mineral. Petrol.*. doi: 10.1007/s00410-004-0639-2

Whitney, J. A., & Stormer, J. C. (1985). Mineralogy, petrology, and magmatic conditions from the fish canyon tuff, central san juan volcanic field, colorado. *Journal of Petrology*, *26*(3), 726–762.

Zellmer, G., Sparks, R., Hawkesworth, C., & Wiedenbeck, M. (2003). Magma emplacement and remobilization timescales beneath montserrat: insights from sr and ba zonation in plagioclase phenocrysts. *Journal of Petrology*, *44*(8), 1413–1431.